

Crop Row Switching for Vision-Based Navigation: A Comprehensive Approach for Efficient Crop Field Navigation

Rajitha de Silva¹, Grzegorz Cielniak² and Junfeng Gao³

Abstract—Vision-based mobile robot navigation systems in arable fields are mostly limited to in-row navigation. The process of switching from one crop row to the next in such systems is often aided by GNSS sensors or multiple camera setups. This paper presents a novel vision-based crop row-switching algorithm that enables a mobile robot to navigate an entire field of arable crops using a single front-mounted camera. The proposed row-switching manoeuvre uses deep learning-based RGB image segmentation and depth data to detect the end of the crop row, and re-entry point to the next crop row which would be used in a multi-state row switching pipeline. Each state of this pipeline use visual feedback or wheel odometry of the robot to successfully navigate towards the next crop row. The proposed crop row navigation pipeline was tested in a real sugar beet field containing crop rows with discontinuities, varying light levels, shadows and irregular headland surfaces. The robot could successfully exit from one crop row and re-enter the next crop row using the proposed pipeline with absolute median errors averaging at 19.25 cm and 6.77° for linear and rotational steps of the proposed manoeuvre.

I. INTRODUCTION

The integration of robotics and autonomous systems in agriculture has enabled precision farming operations leading to effective use of time and resources. Achieving autonomous navigation in agricultural robots is an enabling technology that must be optimised for the deployment of autonomous robots for precision agriculture. The existing autonomous navigation solutions for in-field navigation, albeit being efficient, often relies on expensive sensors such as Real-Time Kinematic Global Navigation Satellite System (RTK-GNSS) sensors. Camera-based agricultural robot navigation systems are a popular alternative to these expensive sensors [1]. Implementation of such vision systems is often limited to crop row following behaviour [2]. In most such systems, row switching is achieved by the aid of GNSS sensors or multiple cameras to identify row end and re-entry to the next row [1], [3], [4].

The premise of vision-based navigation in agricultural robots is to reduce the cost of the overall robotic system with the aim of increased adoption of such technologies. To this end, a vision-based navigation system that uses a single front-mounted camera to perform in-row navigation and row switching would be in line with this objective. In our previous work, we have developed a vision-based crop row

This work was supported by Lincoln Agri-Robotics as part of the Expanding Excellence in England (E3) Programme.

¹Rajitha de Silva, ²Grzegorz Cielniak and ³Junfeng Gao are with Lincoln Agri-Robotics Centre, Lincoln Institute for Agri-Food Technology, University of Lincoln, UK (correspondence author: Junfeng Gao) ¹rajitha@ieee.org, ²gcielniak@lincoln.ac.uk, ³jugao@lincoln.ac.uk

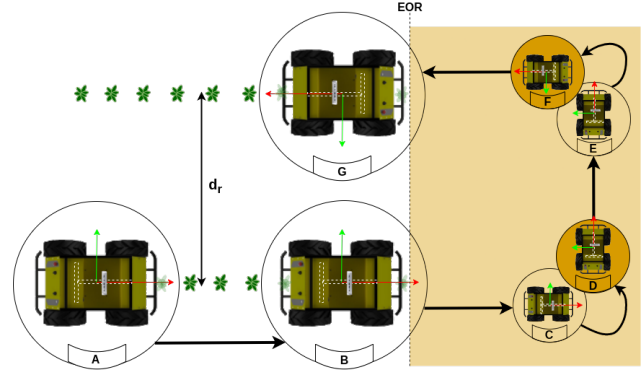


Fig. 1: Crop row switching state machine. d_r : Distance between current and next crop row, A: Initial Detection of the EOR, B: Robot is at the EOR, C: Robot traversed a distance equal to its length into the headland, D: Robot turn 90° towards the next row direction from state C, E: Robot traverse d_r distance forward from state D, F: Robot turn 90° towards the next row direction from state E, G: Robot re-enter the next crop row.

detection algorithm [5] and an in-row navigation framework [6] that then uses the crop row detection to guide the robot through a single crop row only based on RGB images. The crop row switching algorithm presented in this paper relates to our previous work on vision-based crop row detection [5] and navigation [6] in arable fields. The newly proposed algorithm serves as a vital bridge, seamlessly connecting with the established in-row navigation algorithm to dexterously integrate into a comprehensive, fully autonomous field-scale navigation behaviour. This row-switching algorithm could also integrate seamlessly with any other existing in-row navigation methods to eliminate the need for GNSS sensors in row-switching. This existing system can follow a crop row based on RGB image input and it can also identify the location of the end of crop rows when the robot is reaching towards the headland area. The crop row switching algorithm presented is triggered upon the detection of the end of row (EOR) and navigates the robot towards the entry point of the next crop row to be traversed.

The main contributions of this work are as follows:

- A vision-based re-entry point detection algorithm that identifies the relative 3D position of the entry point of the adjacent crop row.
- A crop row switching pipeline based on vision and robot wheel odometry to navigate the robot towards the entry

point of the next crop row to be traversed.

- A comprehensive evaluation and validation of an autonomous navigation system in a real arable field with a mobile robot deployed the proposed system.

II. RELATED WORK

Research into vision-based navigation systems for crop row following is an extensively explored subject area [7], [8]. Existing robot navigation technologies for agri-robotics research include GNSS, inertial navigation systems (INS) and light detection and ranging (LiDAR) [9]. Each of these existing systems presents a cost-benefit trade-off which results in a lack of reliable navigation options for an affordable solution in crop row navigation. The vision-based infield navigation technologies available for arable field navigation explores the usage of RGB and depth images to identify the crop rows [1], [10]. The existing systems for such infield navigation mainly uses image segmentation, object detection or image matching methods to identify the crop rows for robot navigation [7]. Despite the considerable interest in vision-based crop row following systems, the presence of reliable vision-based crop row switching algorithms remains limited [2]. Most of the existing vision-based navigation systems depend completely or partially on GNSS, INS or Lidar-based solutions for crop row switching rather than a fully vision-based solution [7]. The crop row switching algorithms proposed in [2], [11], [12] completely rely on the RTK-GNSS-based sensors to perform the crop row switching manoeuvre. However, GNSS-based systems are not considered a simple and straightforward solution for agricultural robot navigation since they also need multiple redundancies in place for effective operation due to multi-path reflections and signal blockage [13]. Some systems also use manual control to perform the headland turn [14]. Fully vision-based solutions in agricultural robot navigation depend on multiple cameras on the robot for maintaining the localisation during the row switching process [15], [16]. The methods that use a single camera also demand special requirements such as variable field of view [17].

End of row (EOR) detection is an important step for any crop row switching algorithm since it serves as the starting point for any crop row switching manoeuvre [6]. The EOR detection scheme proposed in [18] employs image binarisation using classic computer vision methods to calculate the pixel count in binary masks to determine the EOR. However, the pixel count thresholds may vary depending on the stage of the plant growth and these thresholds must be matched to each growth stage when used for the long term. The pixel counts of binary image representing the crop would not yield the spatial localisation of EOR within a given image, while it only generates an EOR trigger based on the image. In contrast, the EOR detection method proposed by authors of [19] uses Cr channel of $YCbCr$ colour space to calculate the position of the EOR within a given image. Such methods pose the advantage of early detection and potential failures due to noisy images in the method presented in [18]. However, such colour-based EOR detection methods are highly susceptible to distortions

caused by external field variations. The advantages of deep learning-based methods in EOR detection outperform such colour-based methods [5], [6]. A 3D point cloud-based row-end detection was introduced in [14] where the EOR is identified by detection of height drop between the plant and the ground within the point cloud. This approach is mostly limited to crops with noticeable height differences relative to the ground level or crops at later growth stages. The novel EOR detection algorithm presented in this paper is based on the deep learning-based crop row detection model from our earlier work [5], considering the limitations of the existing EOR detection methods. Identification of the relative distance between two crop rows is also vital for accurate crop row switching. The distance between two crop rows often referred to as "inter-row distance" is considered as a fixed distance in existing crop row switching methods [3], [20]. The relative position between the current robot pose and the next crop row could vary due to imperfections in planting or due to a slight offset during robot navigation. Therefore, active perception of the relative position of the re-entry point to the next crop row to be traversed is a useful attribute. The re-entry point detection algorithm proposed in this work estimates the relative distance to the next crop row based on crop row segmentation mask from Triangle Scan Method (TSM) [5] and depth data. Such active perception of inter-row space helps to eliminate any potential row-switching failures caused by varying inter-row space or inaccurate positioning of the robotic platform within the currently traversing crop row. Four most common headland turning patterns are semi-circular turn, U-turn, light bulb turn (a.k.a Ω turn) and switch-back turn [11]. The semi circular turn describes a half circle with a constant radius while U-turn describes two quarter circle turns (90°) centered with a linear traversal stage. These methods are typically used in smaller robots with tighter turning radii relative to the inter-row distance [15], [18], [20]. The Ω turn and the switch-back turn are mostly used in robots with constrained maneuverability such as Ackerman steering robots or tractors [11], [21], [22]. Considering the skid-steering robot configuration of the robotic platform used in this work, U-turn pattern was chosen to execute the row switching manoeuvre.

III. METHODOLOGY

Figure 1 portrays a state machine representing the process of crop row switching, spanning across a total of seven states. Table I describe each state of the process given in Figure 1 encountered during row switching manoeuvre. The robot was driven within the crop rows using Triangle Scan Method (TSM) based crop row navigation framework [6] we have developed in our previous work up to state A . The switching manoeuvre is composed of three steps: row exit, U-turn and re-entry. The transitions $A \rightarrow B \rightarrow C$ belong to the step of row exit. The U-turn step contains to the transitions $C \rightarrow D \rightarrow E \rightarrow F$ while the transition $F \rightarrow G$ is considered as re-entry step. The methods and techniques used in each of these three steps are explained in sections III-B, III-C and III-D respectively.

TABLE I: States encountered during crop row switching manoeuvre.

State	Description
<i>A</i>	Position of the robot during initial EOR detection.
<i>B</i>	Robot reaches the EOR position.
<i>C</i>	Robot enters the headland area completely passing EOR position.
<i>D</i>	Robot turns 90° towards the direction of next crop row from state <i>C</i> .
<i>E</i>	Robot aligns itself with the next crop row traversing forward from state <i>D</i> .
<i>F</i>	Robot turns 90° facing itself towards the starting point of the next crop row while residing within the headland buffer.
<i>G</i>	Robot enters the next crop row.



Fig. 2: Hexman Mark-1 robot in the Sugar Beet Field.

A. Robotic Platform

A Mark-1 robot from Hexman Robotics was used to test the proposed crop row switching algorithm. Figure 2 shows the robotic setup with a front mounted Intel RealSense D435i camera and a Reach RS+ RTK GNSS receiver. A NVIDIA Jetson AGX Orin developer kit was used as the onboard computer for the robot. Mark-1 is a skid steer robot with a ground clearance of 128 mm. The dimensions of the robot are $526 \times 507 \times 244$ mm.

B. Row Exit Step

Row exit is the process in which the robot drives itself completely out of the currently traversing crop row after detecting the EOR. The EOR is initially detected at state *A* where the robot estimates the relative 3D coordinate of the starting point of the next crop row robot would enter. The *Y* value of this relative 3D coordinate would represent the inter-row distance d_r between current and the next crop row. The d_r value is useful when robot is traversing during the $D \rightarrow E$ transition. The robot transits through the states $A \rightarrow B \rightarrow C$ after the re-entry point detection using a combination of visual feature matching and odometry as explained in following subsections.

1) *Re-entry Point Detection*: The re-entry point detection module is extended based on the TSM crop row detection

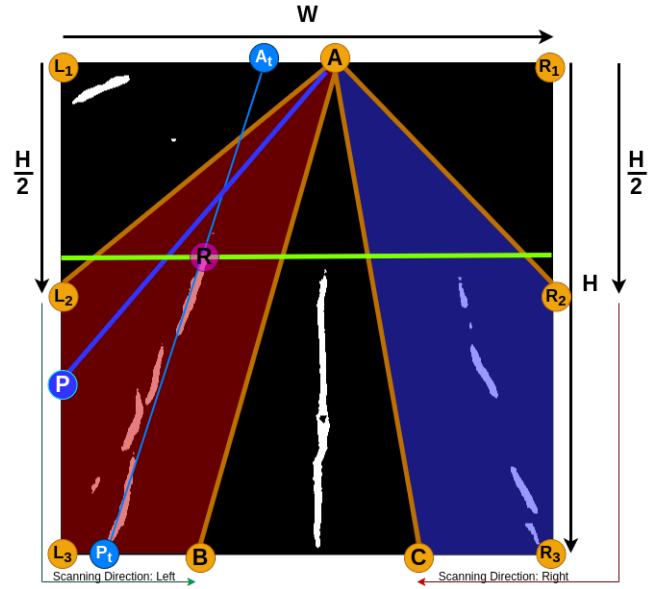


Fig. 3: Regions of interests (ROI) for re-entry point scanning. Red: Left side ROI, Blue: Right side ROI, Green: Detected EOR line.

pipeline from our previous work [5] on crop row detection. Similar to TSM, a deep learning based skeleton segmentation of crop rows was used as the input for the re-entry point detector. As illustrated in Figure 3, the ROI AL_2L_3B was defined if the next intended turn is to the left (AR_2R_3C for right). Points *A*, *B* and *C* were determined using the "Anchor scans" step of TSM [5]. The horizontal green line in Figure 3 was obtained using the EOR detector [6]. Equation 1 yields a point P_t by scanning for the pixel sum along AP line where point *P* is an arbitrary point on L_2L_3B path. Similarly, equation 2 yields a point A_t by scanning the pixel sum along $\bar{A}P_t$ line where point \bar{A} is an arbitrary point on AL_1 line. The intersection between the EOR line and A_tP_t is identified as the re-entry point *R* for the next crop row. The depth information from the corresponding depth image was used to determine the 3D coordinate corresponding to the point *R* which was then used to determine d_r .

$$P_t = \arg \max \left[\sum_{I_{xy}=A}^P I(x, y) \right]_{P=L_1 \rightarrow L_2}^{P=L_2 \rightarrow B} \quad (1)$$

$$A_t = \arg \max \left[\sum_{I_{xy}=P_t}^{\bar{A}} I(x, y) \right]_{\bar{A}=A}^{\bar{A}=L_1} \quad (2)$$

2) *A to B Transition*: The TSM based crop row navigation framework from our previous work [6] was proven to be able to maintain the average heading of the robot relative to the crop row under 1° . Therefore, the relative heading angle between the robot and the crop row was assumed to be under 1° at state *A*. The detected EOR line in Figure 3 demarcates the headland area and the crop row region within the RGB image obtained from the front mounted camera. The

RGB image was cropped below the EOR line and saved as a reference image I_R at state A . The robot was then moved towards the EOR with a constant forward linear velocity while calculating the local feature (Scale Invariant Feature Transform [23] was used) similarity score in each new image captured by the robot camera with I_R . The robot was stopped and assumed to reach state B when the feature similarity score dropped below a experimentally determined threshold. The threshold value was determined by observing the feature similarity score while driving the robot to the actual EOR position using teleoperation.

3) *B to C Transition*: The frontmost edge of the robot is coincident with EOR at state B . The minimum distance the robot must move in order to completely exit the crop row is the length of the robot (L_R) itself. The wheel odometry of the robot was used as feedback to move the robot forward towards the headland. The length of the Hexman Mark 1 robotic platform used in during the field trials was 526 mm. The wheel odometry of the robot was assumed to be accurate enough to navigate the robot forward into the headland at such small distances.

C. U-Turn Step

The U-turn step involves the robot taking two 90° turns with a linear navigation stage ($D \rightarrow E$) in between. "Headland buffer" region is the space in the headland that is directly in front of a given crop row bound by the EOR, edge of the field and the two centre lines of the inter-row space between adjacent crop rows. The goal of the U-turn step is to bring the robot into the headland buffer region of the next crop row while facing towards the next crop row to be traversed. It was experimentally verified that the TSM can resume its normal crop row navigation framework from this point (state F) onward to traverse in to the crop row. The 90° turns and $D \rightarrow E$ transition is executed with wheel odometry feedback of the robot. The practical behaviour of the robot during rotation stages ($C \rightarrow D$ and $E \rightarrow F$) ensured that the robot would reach the headland buffer when the $D \rightarrow E$ transition distance was set to d_r .

D. Re-Entry Step

The robot is within the headland buffer region at state F and state G is reached when the robot enters the next crop row to be traversed. The re-entry step is the transition from state F to state G where the robot moves from the headland buffer into the crop row in front of it. This transition was realized by launching the TSM based crop row following framework at state F . The TSM was able to detect the crop row in front of the robot and navigate the robot into the crop row. This behaviour of TSM based re-entry navigation is verified by the experiment outlined in Section IV-C.

IV. RESULTS AND DISCUSSION

The row switching manoeuvre presented in this paper is a three-step process that involves 6 state transitions as illustrated in Figure 1. The accuracy and the performance

TABLE II: Linear and angular errors during each transition of the row switching maneuver.

Transition	Median Errors		α
	Error	Absolute Error	
$A \rightarrow B$	23.40 cm	31.63 cm	40.20 %
$B \rightarrow C$	8.87 cm	8.87 cm	15.24 %
$C \rightarrow D$	-1.09°	6.91°	-2.88 %
$D \rightarrow E$	12.47 cm	17.26 cm	21.41 %
$E \rightarrow F$	2.51°	6.62°	6.64 %

of each transition is individually evaluated during the experiments. The Hexman Mark-1 robot was programmed to follow a crop row and automatically detect the EOR and re-entry positions. The proposed row-switching manoeuvre is automatically started based on the EOR detection trigger. The path of the robot during the row-switching manoeuvre was tracked using the onboard RTK GNSS tracker with sub-centimeter accuracy.

An experiment was set up in a selected area of 10 crop rows within a real sugar beet field. The GNSS coordinates of the 10 crop rows were recorded with sub-centimetre accuracy by driving the robot through each crop row at very slow speeds by an expert human driver. These ground truth GNSS coordinates of each crop row was then used to generate a regression line which would be used as a reference to calculate errors in autonomous navigation during row switching manoeuvre of the robot. The robot was allowed to autonomously execute the row switching manoeuvre among the 10 crop rows turning in both directions (left and right turns). A total of 18 row-switching trials were conducted during this experiment as plotted in Figure 5. The GNSS coordinates were converted to Universal Transverse Mercator (UTM) coordinates for plotting and error calculations. The errors during each state transition of each row switching manoeuvre trial are illustrated in Figure 4.a where distance errors and angular errors are normalized within a scatter plot. There are 9 x-ticks in Figure 4.a between each pair of adjacent states which represents a pair of consecutive real-world crop rows where the trial took place. A box and whisker plot of the errors for each transition is denoted in Figure 4.b. This normalised representation provides a comparative illustration of the error magnitudes in each state transition. The plots corresponding to translational steps stands above the zero line while box and whisker plots of angular transitions are centered close to zero. Table II presents the median errors of traversal during each stage of the row-switching manoeuvre. Normalized median percentage error ($\alpha = E_{median}/E_{max,T}$) was calculated where $E_{max,T}$ is the maximum absolute error for the type T (T being a distance or an angle) across the entire manoeuvre and E_{median} is the median error for each transition. The vision based transition $A \rightarrow B$ records the highest α value representing the transition with highest error. The remaining transitions record relatively lower α values representing accurate navigation relative to the vision-based transition.

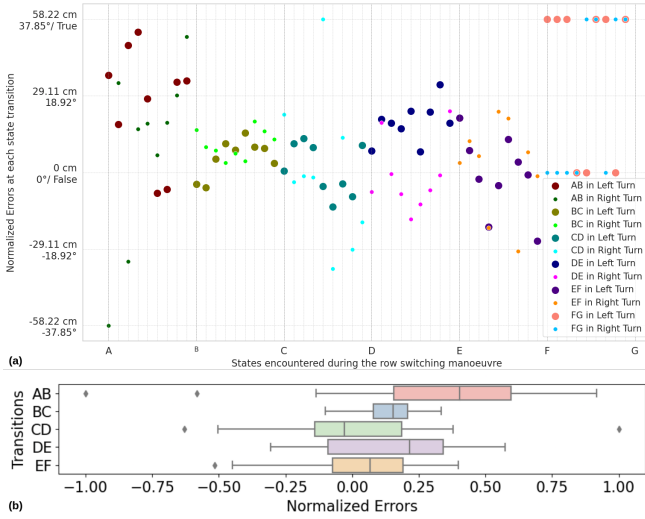


Fig. 4: Normalized state transition errors during the row switching manoeuvre. a: Scatter plot, b: Box and whisker plot.

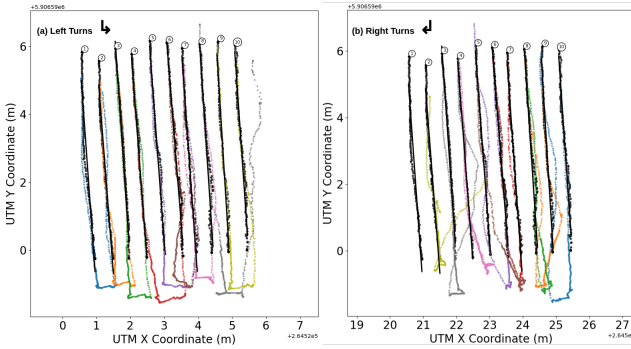


Fig. 5: UTM projections of the GNSS trajectories from row switching experiments (Black: Regression lines and ground truth coordinates).

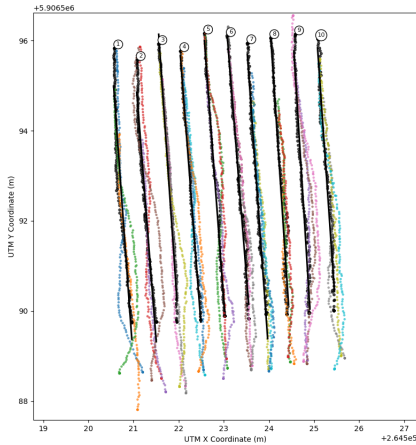


Fig. 6: GNSS trajectories from re-entry experiment (Black: Ground truth coordinates).

A. Crop row exit and headland entry

The row exit step ($A \rightarrow B \rightarrow C$) in the proposed row switching manoeuvre could be identified with the densely distributed GNSS coordinates in Figure 5 leading towards headland from within the crop row in each trial. The dense distribution of GNSS coordinates attributes to the slower speed of row switching manoeuvre relative to the in-row navigation speed of the crop row navigation algorithm.

The row crop row exit ($A \rightarrow B$ transition) is a vision-based navigation stage where the headland entry ($B \rightarrow C$ transition) uses the wheel odometry to guide the robot into the headland area. This difference in feedback modalities is reflected in the distance errors of each transition. The visual feedback in $A \rightarrow B$ transition ensures that the robot has successfully reached the EOR position with visual confirmation. Therefore, it is vital for successfully reaching the EOR despite the higher error margins compared to wheel odometry. Majority of the errors in $A \rightarrow B$ and $B \rightarrow C$ transitions are positive, which indicates that the robot always travel further into the headland area beyond desired positions at states B and C . This trend doesn't have significantly adverse impact on the overall row switching manoeuvre since such extra distance traversed into the headland wouldn't cause the robot to damage crops during the U-turn step.

The robot would stop at 52.6 cm (L_{robot}) away from the actual EOR position in an ideal C state. However, the overall maximum error in the row exit step ($E_{ABC,max}$) was recorded as 64.27 cm, a distance which the robot would move further away from the desired position at state C . Based on these observations, the minimum width $W_{H,min}$ for the headland space was calculated to be 143.17 cm using Equation 3. The coefficient of L_{robot} term in Equation 3 was set to 1.85 since the RTK-GNSS receiver used to measure the robot motion was mounted at 45 cm behind the front of the robot. This coefficient must be changed to $(1 + R)$ where R depends on the position of the RTK-GNSS receiver on the robot, if this experiment is being repeated on a different robot. The robot was expected to be aligned with the crop row at state A within a heading error margin of 2° . A heading error beyond 2° at state A leads the robot to cross into the headland buffer of an adjacent crop row at state C , which would cause it to skip 1 crop row during switching or re-enter to the same crop row it traversed as seen in the unsuccessful attempts in Figure 5.

$$W_{H,min} = 1.85 \times L_{robot} + E_{ABC,max} \quad (3)$$

B. U-turn towards next crop row

The U-turn step of the row switching manoeuvre is represented by the state transitions $C \rightarrow D \rightarrow E \rightarrow F$. The angular error for $C \rightarrow D$ transition was calculated based on the angle between \overrightarrow{AC} and \overrightarrow{DE} vectors. The angle between \overrightarrow{DE} and $\overrightarrow{FF_N}$ vectors was considered to calculate the angular error for $E \rightarrow F$ transition where F_N is a point on the GNSS trajectory which is $N(=5)$ points after the GNSS coordinate of state F . Distance error for $D \rightarrow E$ transition was calculated by comparing the DE distance with

the inter-row distance between the adjacent crop rows which the robot is being switched, using regressed ground truth lines.

The angular errors in both rotational transitions are evenly distributed with a near zero mean. The absolute median angular errors during rotational transitions were less than 7° . These error margins could be considered as acceptable for this application scenario since such small angular errors wouldn't incur significant deviations to \overrightarrow{DE} and \overrightarrow{FG} vectors. The robot would stay at the same place without any translational motion in an ideal rotational transition. However, it was evident from some of the recorded trajectories in Figure 5 that these rotations also incur some translational motion within the trajectory. Such motions push the robot towards or away from the direction of next crop row. This would cause the robot to skip the next crop row to be traversed or turn towards the same row it came in, despite achieving the desired \overrightarrow{DE} distance. This unintended translational motion is often caused by the uneven terrain in the headland area which is not detected by the wheel odometry. The headland buffer area of 4th crop row had such uneven terrain which lead to failure of both left and right turns originated from that crop row.

C. TSM based Re-Entry Validation

The median error for $D \rightarrow E$ transition which led to successful re-entry was always below 30 cm. This indicate that the robot could execute a successful re-entry when it faces the next crop row with a perpendicular offset of 30 cm or below at state F . An experiment was setup to validate this hypothesis where the robot was placed facing towards the crop row at different angles within the headland buffer of a given crop row. The TSM algorithm was executed on the robot such that it would detect the crop row in front of it and gradually drive the robot into the crop row in front. The path of the robot was recorded in GNSS coordinates as plotted in Figure 6. All the recorded trajectories could successfully enter the row in front of it since the robot was initiated in the headland buffer and facing towards the general direction of the crop row in front of it.

The re-entry failures in Figure 5 could be explained by the main findings of this experiment. There are two key factors governing the success of a re-entry to the next crop row during $F \rightarrow G$ transition. First requirement is that the robot must be positioned within the headland buffer of the crop row it intends to enter. If the perpendicular offset between the crop row and robot position at state F is beyond 30 cm, a re-entry failure occurs. The second factor is that the robot must be oriented towards the general direction of the crop row it intends to enter. Maximum deviation angle of the robot heading from crop row was 26° in the experiment illustrated in Figure 6. Although the errors in individual state transitions of the row switching manoeuvre are minimal, the overall outcome of all transitions would not lead to success when these two requirements are not met at state F .

V. CONCLUSION AND FUTURE WORK

The proposed row-switching manoeuvre could navigate the robot from one crop row to another without needing RTK-GNSS sensors or multiple cameras while using a single front mounted camera on the robot. Individual steps of the row-switching manoeuvre demonstrated excellent results within the context of each state transition and its functionality. The vision-based $A \rightarrow B$ transition was the transition with highest errors in the proposed manoeuvre. The rotational transitions of the manoeuvre yielded smaller percentage errors relative to the translational transitions. The success rate of the conducted row switching experiment was 55.5% while the re-entry experiment yielded 100% success rate. The row switching manoeuvre is also crop agnostic since it doesn't rely on plant specific visual features.

Two main unexpected behaviour patterns in the row exit and U-turn steps lead to the failure of row switching: large heading error at state A and translational motion during rotational state transitions. These two shortcomings of the proposed row switching manoeuvre could be corrected by introducing a heading correction step at state A and inertial measurement unit (IMU) based sensor fusion to track the unintended translational motion during the rotational transitions correcting the intended \overrightarrow{DE} distance.

REFERENCES

- [1] S. Bonadies and S. A. Gadsden, "An overview of autonomous crop row navigation strategies for unmanned ground vehicles," *Engineering in Agriculture, Environment and Food*, vol. 12, no. 1, pp. 24–31, 2019.
- [2] P. Huang, Z. Zhang, and X. Luo, "Feedforward-plus-proportional-integral-derivative controller for agricultural robot turning in headland," *International Journal of Advanced Robotic Systems*, vol. 17, no. 1, p. 1729881419897678, 2020.
- [3] A. Ahmadi, L. Nardi, N. Chebrolu, and C. Stachniss, "Visual servoing-based navigation for monitoring row-crop fields," in *2020 IEEE International Conference on Robotics and Automation (ICRA)*. IEEE, 2020, pp. 4920–4926.
- [4] S. Kanagasingham, M. Ekpanyapong, and R. Chaihan, "Integrating machine vision-based row guidance with gps and compass-based routing to achieve autonomous navigation for a rice field weeding robot," *Precision Agriculture*, vol. 21, no. 4, pp. 831–855, 2020.
- [5] R. de Silva, G. Cielniak, G. Wang, and J. Gao, "Deep learning-based crop row detection for infield navigation of agri-robots," *Journal of Field Robotics*, 2023.
- [6] R. de Silva, G. Cielniak, and J. Gao, "Vision based crop row navigation under varying field conditions in arable fields," *arXiv preprint arXiv:2209.14003*, 2022.
- [7] T. Wang, B. Chen, Z. Zhang, H. Li, and M. Zhang, "Applications of machine vision in agricultural robot navigation: A review," *Computers and Electronics in Agriculture*, vol. 198, p. 107085, 2022.
- [8] N. Shalal, T. Low, C. McCarthy, and N. Hancock, "A review of autonomous navigation systems in agricultural environments," *SEAG 2013: Innovative agricultural technologies for a sustainable future*, 2013.
- [9] Z. Man, J. Yuhan, L. Shichao, C. Ruyue, X. Hongzhen, and Z. Zhenqian, "Research progress of agricultural machinery navigation technology," *Nongye Jixie Xuebao/Transactions of the Chinese Society of Agricultural Machinery*, vol. 51, no. 4, 2020.
- [10] Y. Bai, B. Zhang, N. Xu, J. Zhou, J. Shi, and Z. Diao, "Vision-based navigation and guidance for agricultural autonomous vehicles and robots: A review," *Computers and Electronics in Agriculture*, vol. 205, p. 107584, 2023.
- [11] Z. He, Y. Bao, Q. Yu, P. Lu, Y. He, and Y. Liu, "Dynamic path planning method for headland turning of unmanned agricultural vehicles," *Computers and Electronics in Agriculture*, vol. 206, p. 107699, 2023.

- [12] D. S. Paraforos, R. Hübner, and H. W. Griepentrog, "Automatic determination of headland turning from auto-steering position data for minimising the infield non-working time," *Computers and electronics in agriculture*, vol. 152, pp. 393–400, 2018.
- [13] F. Rovira-Más, I. Chatterjee, and V. Sáiz-Rubio, "The role of gnss in the navigation strategies of cost-effective agricultural robots," *Computers and electronics in Agriculture*, vol. 112, pp. 172–183, 2015.
- [14] J. Kneip, P. Fleischmann, and K. Berns, "Crop edge detection based on stereo vision," *Robotics and Autonomous Systems*, vol. 123, p. 103323, 2020.
- [15] A. Ahmadi, M. Halstead, and C. McCool, "Towards autonomous visual navigation in arable fields," in *2022 IEEE/RSJ International Conference on Intelligent Robots and Systems (IROS)*. IEEE, 2022, pp. 6585–6592.
- [16] E. Liu, J. Monica, K. Gold, L. Cadle-Davidson, D. Combs, and Y. Jiang, "Vision-based vineyard navigation solution with automatic annotation," *arXiv preprint arXiv:2303.14347*, 2023.
- [17] J. L. Xue and T. E. Grift, "Agricultural robot turning in the headland of corn fields," *Applied Mechanics and Materials*, vol. 63, pp. 780–784, 2011.
- [18] P. Huang, L. Zhu, Z. Zhang, and C. Yang, "Row end detection and headland turning control for an autonomous banana-picking robot," *Machines*, vol. 9, no. 5, p. 103, 2021.
- [19] Z. Zhang, R. Cao, C. Peng, R. Liu, Y. Sun, M. Zhang, and H. Li, "Cut-edge detection method for rice harvesting based on machine vision," *Agronomy*, vol. 10, no. 4, p. 590, 2020.
- [20] L. Guevara, M. M. Michalek, and F. A. Cheein, "Headland turning algorithmization for autonomous n-trailer vehicles in agricultural scenarios," *Computers and Electronics in Agriculture*, vol. 175, p. 105541, 2020.
- [21] H. Wang and N. Noguchi, "Adaptive turning control for an agricultural robot tractor," *International Journal of Agricultural and Biological Engineering*, vol. 11, no. 6, pp. 113–119, 2018.
- [22] J. T. Evans IV, S. K. Pitla, J. D. Luck, and M. Kocher, "Row crop grain harvester path optimization in headland patterns," *Computers and electronics in agriculture*, vol. 171, p. 105295, 2020.
- [23] D. G. Lowe, "Distinctive image features from scale-invariant keypoints," *International journal of computer vision*, vol. 60, pp. 91–110, 2004.